On the Comparison of Different Methods for Impedance Eduction Applied to a Numerical Database

On the comparison of different methods for impedance eduction applied to a numerical database

Francesco Avallone *, Angelo Paduano†
Politecnico di Torino, Corso Duca degli Abruzzi 24, 10122, Torino, Italy

Lucas M. Pereira‡, Lucas A. Bonomo §, Julio A. Cordioli¶
Federal University of Santa Catarina, Florianópolis - SC, 88040-900, Brazil

Damiano Casalino‖
Delft University of Technology, Kluyverweg 1, 2629HS, Delft

Davide Cerizza **
Dassault Systemes – SIMULIA, Waltham MA, 02451, USA

Eduction methods are adopted to characterize acoustic liners. In this paper, several impedance eduction techniques are compared using a numerical database obtained with scale resolved lattice-Boltzmann simulations of a reference acoustic liner in the presence or not of a grazing turbulent flow. Three impedance eduction techniques are compared: an inverse approach based on the Mode-Matching (MM) method, the straightforward method based on the Prony-like Kumaresan-Tufts (KT) algorithm, and one approach based on a minimization problem between reference measurements and the solution of the Pierce's equation. Furthermore, the educed impedance is compared with the one obtained using local impedance measurements with the Dean's method with virtual probes located on the entire face-sheet. Results show that impedance values obtained with the Deans' method are highly dependent on the sampling location and that they vary largely over each cavity. Results from the eduction methods are similar amongst them with few discrepancies found for the method based on the Pierce's equation. In particular, the highest value of resistance obtained using the Deans' method is similar to the one obtained using the KT and MM eduction methods.

I. Introduction

Aircraft noise is of great concern, particularly near airports. Among the various noise sources, the most prominent one is generated by the engines, especially by the fan in Ultra High Bypass Ratio (UHBR) engines. They are characterized by a larger fan diameter, a shorter nacelle, a lower rotational speed of the fan, and a lower jet core velocity with respect to conventional HBR engines. Fan noise in turbofan engines is characterized by tonal components at harmonics of the Blade-Passage Frequency (BPF) and broadband components mostly caused by the interaction between the turbulent wake from the rotor and the stator, especially in proximity of the shroud where the velocity fluctuation levels are higher [1]. Acoustic liners are the state-of-the-art technology to reduce engine noise.

In-use aero-engine acoustic liners are passive devices comprised of panels featuring a sandwich structure, which generally includes a honeycomb core sandwiched between a perforated face-sheet and a solid backplate. This design is commonly referred to as a Single Degree of Freedom (SDOF) liner. An acoustic liner is characterized by its acoustic impedance $\tilde{Z}/Z_o = \theta + i\chi$, where θ is named resistance and χ reactance, while $Z_0 = \rho_0 c_0$ is the characteristic acoustic impedance of air.

A large effort has been dedicated in developing experimental techniques to measure the acoustic impedance [2–10].

*Full Professor, Department of Mechanical and Aerospace Engineering, francesco.avallone@polito.it, AIAA member.
†PhD student, Department of Mechanical and Aerospace Engineering, angelo.paduano@polito.it.
‡PhD student, Department of Mechanical Engineering, lucas.meirelles@lva.ufsc.br, AIAA member.
§PhD student, Department of Mechanical Engineering, lucas.bonomo@lva.ufsc.br, AIAA member.
¶Associate Professor, Department of Mechanical Engineering, julio.cordioli@ufsc.br, AIAA member.
‖Full Professor, Department of Flow Physics and Technology, d.casalino@tudelft.nl, AIAA member.
**Software Engineering Manager, SIMULIA R&D, Fluids Science & Technology, davide.cerizza@3ds.com.

Focus has been given to develop approaches that can be used to measure impedance when the acoustic absorbing surface is grazed by a turbulent flow and high amplitude acoustic waves, such as in realistic operating flight conditions.

Impedance eduction methods can be divided in direct and inverse methods [11]. Direct methods use an estimation of the axial wavenumber in conjunction with an impedance boundary condition to educe impedance without iterations [4, 7, 12]. Inverse methods, on the other hand, solve a minimization problem by minimizing the difference between the measured acoustic pressure [4, 6, 11, 13–15], and the one obtained by solving a partial differential equation with an impedance boundary condition, that can account or not for shear flow effect [16]. It has been shown that similar results are obtained by using direct or inverse eduction methods, but discrepancies still exist [17].

When using eduction methods, a boundary condition is needed to model the liner. The most widely adopted boundary condition is the Ingard-Myers [18, 19], which is used to model the effect of a non-uniform mean flow on the acoustic propagation in the immediate vicinity of a sound absorbing surface. This is achieved by enforcing continuity of acoustic displacement across an infinitely thin inviscid boundary layer to the first order. The effective impedance obtained using this approach depends on the wavenumber, frequency, Mach bulk velocity and the actual normalized impedance of the treated surface. Therefore, the effective impedance is non-locally reacting, and depends on the wavenumber. The Ingard-Myers boundary conditions, as it was proposed, is ill-posed. Khamis et al. [20] have corrected this behaviour by introducing the effect of viscosity and obtained a novel boundary condition accurate to the second order. This boundary condition assumes that the boundary layer over the lined surface is weakly altered with respect to a smooth wall, but this is not always true as experimentally demonstrated by Léon et al. [21] and particularly not true when considering a bulk liner.

The method proposed by Dean [10], based on the measurements of unsteady pressure fluctuations both at the face-sheet and backplate, can be used to avoid the use of boundary conditions as the one described previously. However, impedance obtained with the Dean's method depends largely on the location of the microphone at the face-sheet. Furthermore, it is experimentally challenging to install the microphones and assure that there is not leakage after installation. Therefore, the number of microphones adopted is very limited [22].

Despite the substantial number of published articles on impedance eduction techniques, there is a scarcity of direct comparisons. Recently, the International Forum for Aviation Research (IFAR) initiated a collaborative project with the objective of addressing this gap [23, 24]. The first challenge under the IFAR liner topic involved collecting data from multiple test rigs utilizing simple liner configurations feasible for construction using 3D printing technology. However, the precision and surface finishing of 3D printing equipment can vary significantly, raising concerns about sample uniformity due to anticipated manufacturing process disparities [23]. Additionally, differences in test rig geometries and flow supply systems likely resulted in distinct flow profiles at each rig, aspects that were not assessed in the aforementioned study.

In this paper, impedance values obtained with different methods are compared using a numerical database obtained using the Lattice-Boltzmann/Very Large Eddy Simulation (LB/VLES) solver PowerFLOW® on a reference liner geometry for which experimental data exists [25]. The numerical database consists of cases without and with grazing flow with centerline Mach number equal to 0.32, and tonal excitation at three discrete frequencies and two amplitudes equal to 130 and 145 dB. Furthermore, data with acoustic wave propagating in the same direction and in the direction opposite to the mean flow is available. Impedance values educed using the Mode-Matching (MM) method, the Prony-like Kumaresan-Tufts (KT) algorithm, a method based on a minimization problem between reference measurements and the solution of the Pierce's equation, and calculated with the Dean's method on the entire face-sheet are compared.

II. Liner geometry and testing conditions

The reference acoustic liner is the one described by Bonomo et al. [25]. The geometry was fully characterized using 3D scanning. Details about the flow features within the orifice, and the extensive validation of the numerical simulations are described in a companion paper [26]. A picture of the geometry reconstructed based on the 3D scan is reported in figure 1. The geometrical characteristics of the geometry are summarized in table 1. It is of particular relevance the rounding of the orifice edge with a radius of curvature of about 12% of the face-sheet thickness.

The high-fidelity database consists of the reference liner simulated both in the presence and absence of grazing turbulent flow with a centerline Mach number equal to 0.32. The grazing acoustic wave is a tonal plane wave. Several acoustic waves are investigated: amplitudes equal to 130 dB and 145 dB and frequencies equal to 800 Hz, 1400 Hz and 2000 Hz. In the presence of grazing flow, cases with acoustic waves propagating in the same direction and in the direction opposite to the mean flow are also investigated.

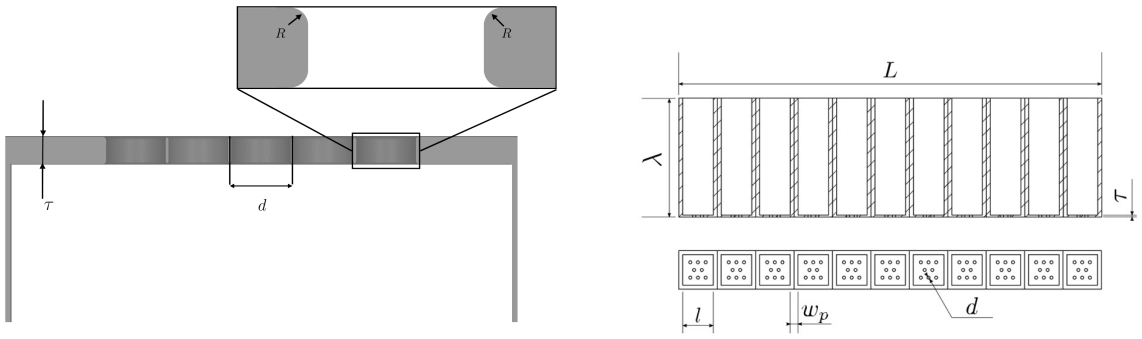

(a) **(b)**

Fig. 1 Liner geometry reconstructed from 3D scanning after manufacturing.

	L	l	τ	w_p	d	λ	R
mm	136.91	9.91	0.54	2.54	1.15	38.1	0.065

Table 1 Geometric parameters of the investigated liner sample.

III. Eduction methods

A. In-situ method

The in-situ technique, also known as the two-microphone method, was first proposed by Dean [10]. It involves measuring unsteady pressure at the face-sheet and at the bottom of the cavity. This method provides a point-wise measurement of impedance. The impedance is computed as:

$$Z_f = \frac{Z}{Z_0} = -i\frac{|p_f|}{|p_b|}e^{i\phi}\frac{1}{\sin(k\lambda)}, \tag{1}$$

where p_f and p_b are the pressure measured at the face-sheet and backplate respectively, ϕ is the phase angle between the surface and backplate pressure measurements and $k = \omega/c_0$ is the free-field wavenumber, with ω being the acoustic wave angular frequency.

B. Mode-matching method

Mode matching is an indirect method of impedance eduction. The main characteristic of the MM method is the match of modal amplitudes at the interfaces between treated and untreated sections [25, 27]. The MM method for impedance eduction was first proposed by Elnady and Bodén [4] and subsequently validated by Elnady [28]. In this work a modified MM method is used, where only plane waves are assumed to propagate. This method involves measurements of pressure before and after the liner. The difference between the pressure complex amplitudes at the microphones location and the theoretical model is minimized. Details about the procedure are reported by Spillere et al. [27] and Bonomo et al. [29].

C. Prony-like Kumaresan-Tufts algorithm

The application of the Prony-line Kumaresan-Tufts algorithm to educe the liner's impedance relies on the acoustic pressure measurement on equally spaced microphones located in the lined section. The algorithm extracts the axial wavenumber of the lined section by assuming the acoustic field can be represented by a sum of damped exponential. Assuming temporal dependence in the form of exp(iωt), the acoustic propagation is governed by the linearized convected Helmholtz equation. Applying the boundary condition proposed by Ingard [18] leads to the eigenvalue problem:

$$\alpha\tan(\alpha H) - \frac{Z_0}{ikZ}(ik - iM\zeta)^2 = 0, \tag{2}$$

where α is the transverse wavenumber, k is the wavenumber and ζ is the axial wavenumber. The dispersion relation is given by:

$$\alpha^2 = (k - M\zeta)^2 - \zeta^2. \tag{3}$$

Once the axial wavenumber is known, it is straightforward to calculate the liner impedance [29].

D. Methods based on the solution of the Pierce equation

This inverse impedance eduction method is based on solutions of wave equations in the frequency domain by means of the FEM solver *Opty∂B*-GFD. Two wave propagation models are adopted in the FEM solver. One is a standard 2nd order wave model based on the Pierce's equation for the acoustic velocity potential [30–33], and the other one is a 3rd order wave model based on the Lilley's equation for the pressure perturbation [34–36]. Comparative studies between these two models for duct acoustics problems in the presence of acoustically treated walls were presented by Casalino et al. [37, 38]. The Pierce equation models the lined wall using an Ingard-Myers impedance boundary condition. Two approaches have been tested for determining the mean-flow velocity: one involves extracting it from the time-average CFD solution starting at a distance equal to the height of the first cell of the FEM mesh, while the other relies on a wall-normal uniform flow based on input flow conditions. The FEM simulations are performed using the SIMULIA liner impedance reduction workflow [36].

IV. Results

A. Grazing acoustic wave without grazing turbulent flow

The analysis for the case without grazing flow starts with the spatial distribution of the resistance and reactance values obtained by using the Deans' method with virtual probes located on the entire face-sheet. On the other hand, the backplate virtual probe is located at the center of each cavity. The resistance and reactance values are shown in Figures 2 and 3 for acoustic waves with frequency equal to 1400 Hz and both amplitudes. The acoustic wave propagates from the left to the right of the figure. The other two frequencies show similar trends and they are not plotted for the sake of conciseness. The figures show the variation with respect to the mean value calculated over the entire face-sheet. The mean value for each component and case is reported in each subfigure.

In the absence of grazing flow, the impact of the non-linear effects associated to the high amplitude of the acoustic wave are visible with an increase of the mean value of resistance. For both amplitudes, the mean resistance value on each cavity decreases moving in the downstream direction. Furthermore, it can be observed that the resistance decreases across each cavity. Therefore, it can be concluded that the value of resistance obtained using the Deans' method varies with the location of the virtual probe. The reactance values for both amplitudes show a weak increase along the liner sample in the area where the orifices are located, while it shows larger value of impedance at the edges of the sample.

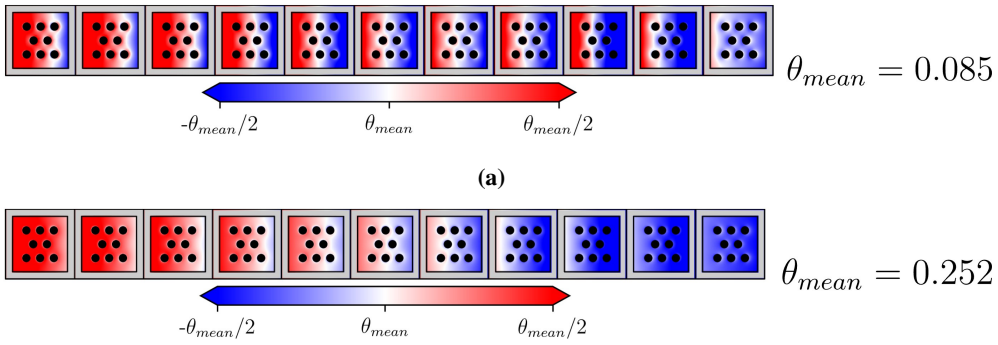

Fig. 2 Contour plots of the resistance component of impedance computed using the Dean's method on the entire liner face-sheet. Tonal plane wave with frequency equal to 1400 Hz and amplitudes equal to (a) 130 dB and (b) 145 dB in absence of grazing flow.

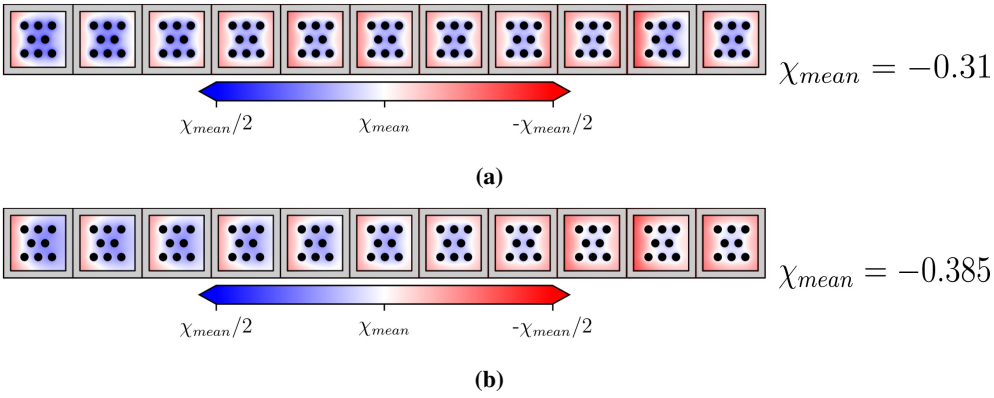

Fig. 3 Contour plots of the reactance component of impedance computed using the Dean's method on the entire liner face-sheet. Tonal plane wave with frequency equal to 1400 Hz and amplitudes equal to (a) 130 dB and (b) 145 dB in absence of grazing flow.

To further quantify the variation of the impedance due to the positioning of the virtual probes, Figures 4 and 5 show line plots of both the resistance and reactance extracted at the face-sheet, slightly below the centerline, i.e., where no orifice is present. For the sake of conciseness only the case with acoustic wave amplitude equal to 145 dB is shown. In each figure, the three frequencies analyzed are reported. The red continuous line shows the computational data extracted by the previous contour plots, the black dot is the average value on each cell, and the blue line is the local predicted value obtained using the semi-empirical model proposed by Yu et al. [39], which accounts for the boundary layer properties and the SPL value at each face-sheet location.

It can be observed that the average resistance along the entire liner sample is almost constant for tonal plane wave with frequency equal to 800 Hz, while it decreases moving downstream for the other two frequencies. This is in agreement with the prediction from the semi-empirical model because it is mainly due to the SPL decay over the liner. The resistance decreases along each cavity for frequencies equal to 800 Hz and 1400 Hz, while it shows a weak increase for the case with tonal plane wave at 2000 Hz. The variation over each cavity decreases with increasing frequency. The difference between prediction from the semi-empirical model and the numerical results decreases when the acoustic wave frequency is equal to 2000 Hz.

Reactance values are almost constant along the liner sample for all the cases, with a small increase for 1400 Hz and 2000 Hz. Reactance values show a local minimum at the center of each cavity, while, for the most upstream cavities, a local maximum at the most upstream edge of each cavity is found. The differences with respect to the values predicted by the semi empirical models are large for all the frequencies.

The analysis continues with the comparison between all the methods introduced previously. Figures 6 and 7 show both components of impedance for acoustic wave amplitude equal to 130 dB and 145 dB, respectively. Resistance and reactance values obtained from both the simulations, experiments [25] and the semi-empirical model [39] are presented. Values obtained with the Dean's method, plotted with symbols, correspond to a virtual probe located on the first cavity at the same location as in the reference experiment. The bar, on the other hand, shows the minimum and maximum values on the entire face-sheet. It is important to observe, that experimental data is obtained on a sample that is longer than the computational one, i.e. the liner tested experimentally was 400 mm long while the one simulated was 136.91 mm long.

For the case with acoustic wave amplitude equal to 130 dB, all the methods show comparable results for both experiments and simulations. The in-situ method shows a decreasing trend at higher frequencies using both numerical and experimental input data. Numerical data shows a slightly lower value of resistance at 800 Hz, maybe because of the short length of the sample. Reactance values, on the other hand, show evident discrepancies between in-situ and eduction methods which are consistent in both numerical simulations and experiments. Values of reactance predicted by the semi-empirical model are very close to the in-situ ones. It is worth to mention that this discrepancy might be due to the relevance of the partition wall thickness for this liner and that by using the approach proposed by Jones and Nark [40] a better agreement with the eduction method is expected.

Increasing the amplitude of the acoustic wave, a larger scatter between the methods is found. Eduction methods show similar results when using as input numerical or experimental data. Local values measured with the in-situ are lower than the reference experiment and also lower that the ones obtained by the other methods. However, the highest

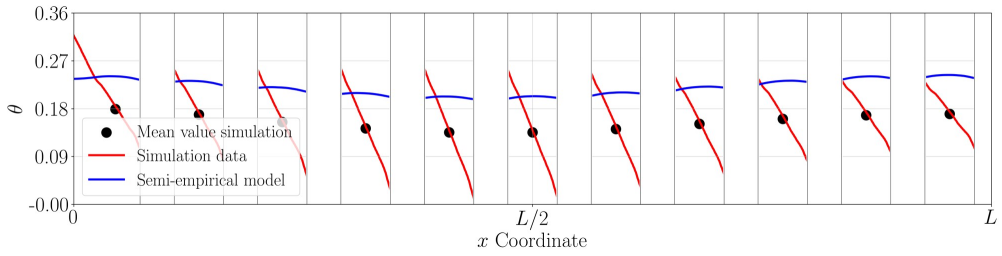

(a)

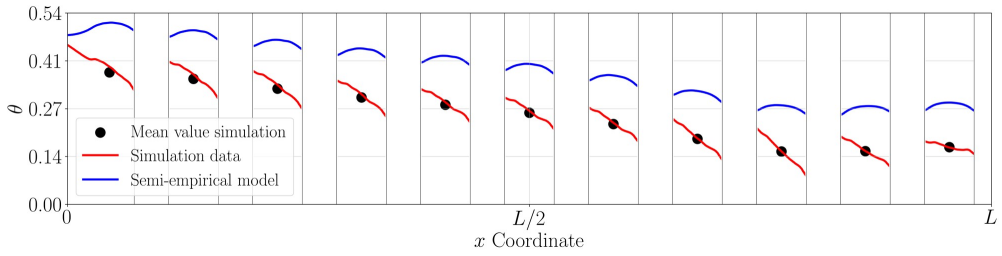

(b)

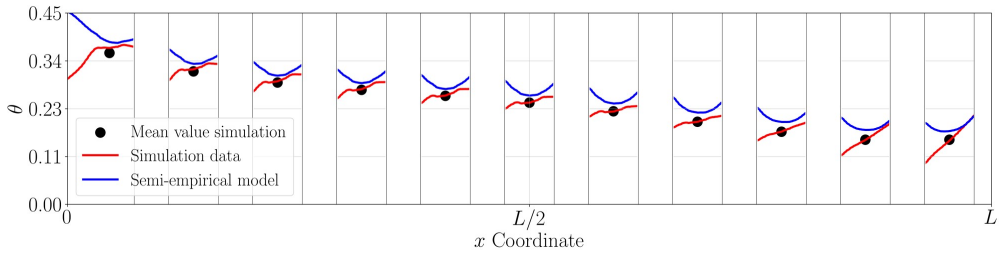

(c)

Fig. 4 Spatial distribution of the resistance component of impedance computed using the Dean's method along the face-sheet centerline. Tonal plane wave with amplitude equal to 145dB and tonal frequency equal to (a) 800 Hz, (b) 1400 Hz and (c) 2000 Hz in absence of grazing flow.

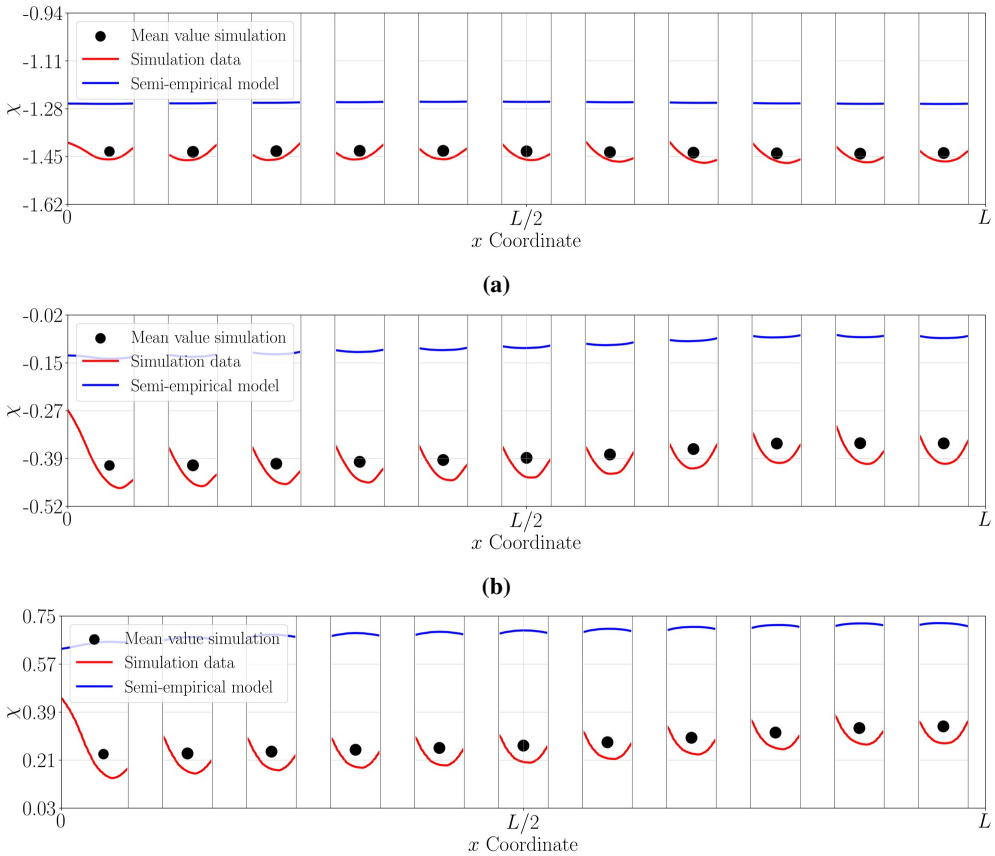

Fig. 5 Spatial distribution of the resistance component of impedance computed using the Dean's method along the face-sheet centerline. Tonal plane wave with amplitude equal to 145dB and tonal frequency equal to (a) 800 Hz, (b) 1400 Hz and (c) 2000 Hz in absence of grazing flow.

values obtained with the Deans' method are close to the one obtained with the eduction methods. Reactance values show very similar trend as the lower amplitude acoustic wave case.

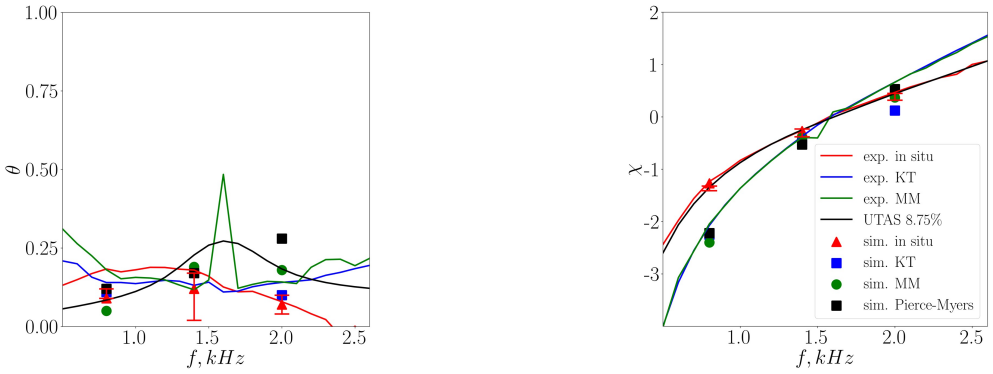

(a) **(b)**

Fig. 6 Comparison of (a) resistance and (b) reactance component of impedance for acoustic wave amplitude equal to 130 dB without grazing flow.

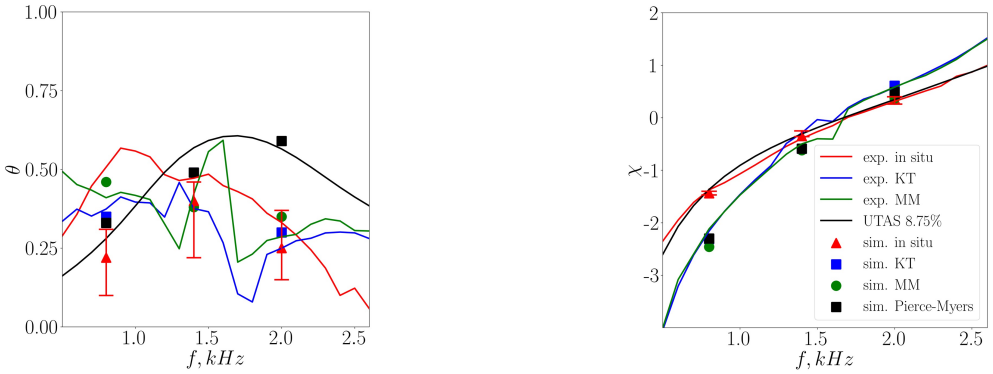

(a) **(b)**

Fig. 7 Comparison of (a) resistance and (b) reactance component of impedance for acoustic wave amplitude equal to 145 dB without grazing flow.

B. Grazing acoustic wave with grazing turbulent flow

The analysis starts with the cases with acoustic wave propagating in the same direction of the mean flow, i.e., from the left to the right in the following figures. Before comparing the different methods in the presence of grazing flow, the surface distribution of impedance obtained using the Dean's method is shown in Figures 8 and 9. For the sake of conciseness, contour plots are shown only for one frequency of the acoustic wave f = 1400 Hz and the two amplitudes analyzed. In the figures, the variation with respect to the surface-averaged mean value is shown to highlight the relevance of the selection of the probe location.

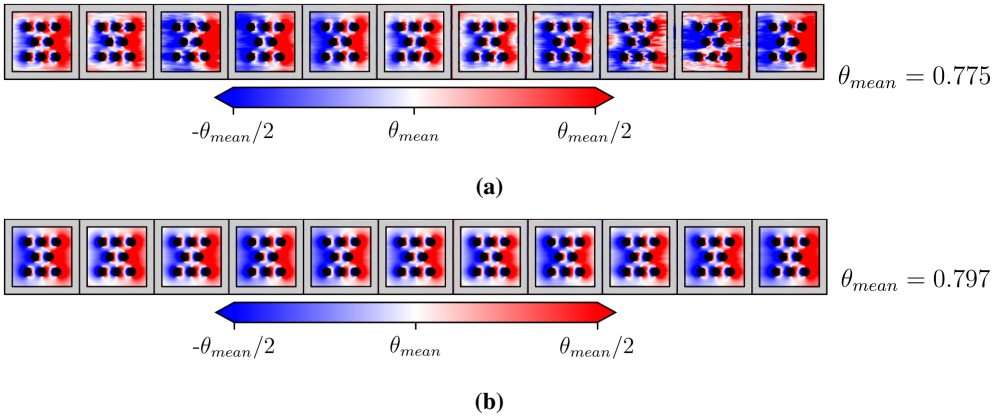

Fig. 8 Contour plots of the resistance component of impedance computed using the Dean's method on the entire liner face-sheet. Tonal plane wave with frequency equal to 1400 Hz and amplitude equal to (a) 130 dB and (b) 145 dB. Turbulent grazing flow with centerline Mach number equal to 0.32.

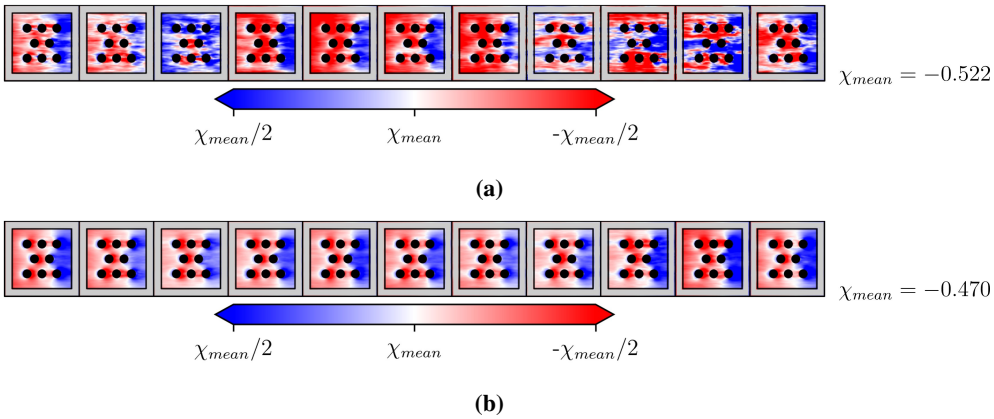

Fig. 9 Contour plots of the reactance component of impedance computed using the Dean's method on the entire liner face-sheet. Tonal plane wave with frequency equal to 1400 Hz and amplitude equal to (a) 130 dB and (b) 145 dB. Turbulent grazing flow with centerline Mach number equal to 0.32.

It is evident that the computed values of both components of impedance vary largely changing the location of the face-sheet virtual probe. For both amplitudes, the pattern is similar. There is an increase of the resistance moving from upstream to downstream of each cavity, and the value of impedance varies weakly with the amplitude of the acoustic wave. However, it is possible to notice that, for the case with acoustic wave amplitude equal to 130 dB there are more fluctuations within each cavity because of the larger impact of the hydrodynamic surface pressure fluctuations with respect to the acoustic ones and the short time series available in order to limit the computational cost. For both cases, it is also relevant to notice that there is a visible effect of the near-orifice flow features. As a matter of fact, impedance decreases upstream of each orifice and increases downstream of it, independently on the orifice location.

A similar trend can be observed when looking at the reactance component of impedance, where a decrease can be

observed moving from upstream to downstream of each cavity. In this case, the effect of the turbulent boundary layer, given also the limited amount of samples available, is more evident on the case with lower acoustic wave amplitude. For the reactance, the impact of the near-orifice flow structures is less relevant with respect to the resistance.

To further quantify the variation due to the positioning of the virtual probes, Figures 10 and 11 show line plots of both resistance and reactance extracted at the face-sheet as already described in the previous section. For the sake of conciseness, also in this case, only the case with acoustic wave amplitude equal to 145 dB is shown. In each figure, the three frequencies analyzed are reported. Lines in the figures are the same as the ones described in the previous section.

Starting from the resistance spatial distribution, it is evident that the computed mean value is lower than the one predicted by the semi-empirical model. However, as also visible previously, the variation of the computed resistance is very large, i.e. $0.5 < \theta < 1.4$, thus highlighting again the impact of the sampling location. It is relevant to notice that the semi-empirical model predicts values of impedance that are on the high-end side of the local value estimated using numerical data. The trend is almost independent on the frequency of acoustic excitation. Similar considerations can be done for the case with amplitude of the acoustic wave equal to 130 dB even if not reported here.

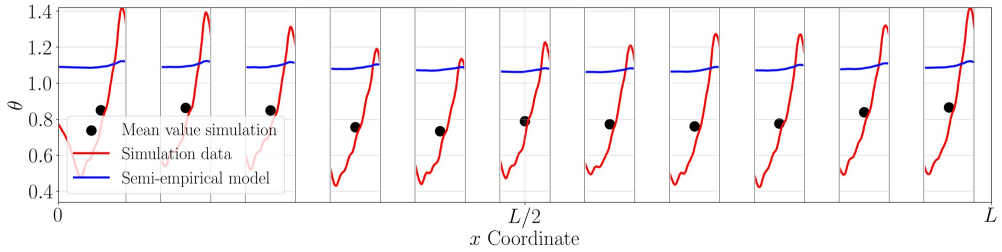

(a)

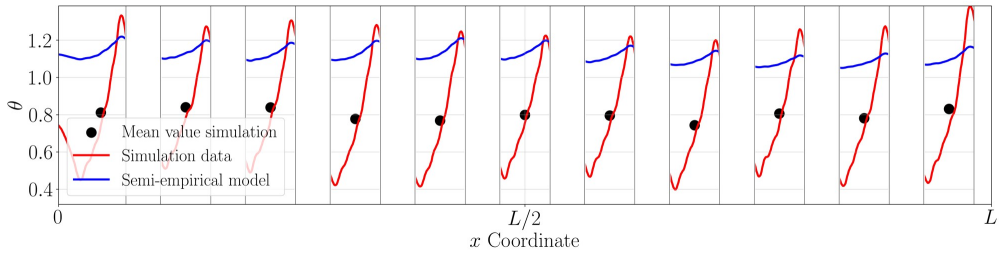

(b)

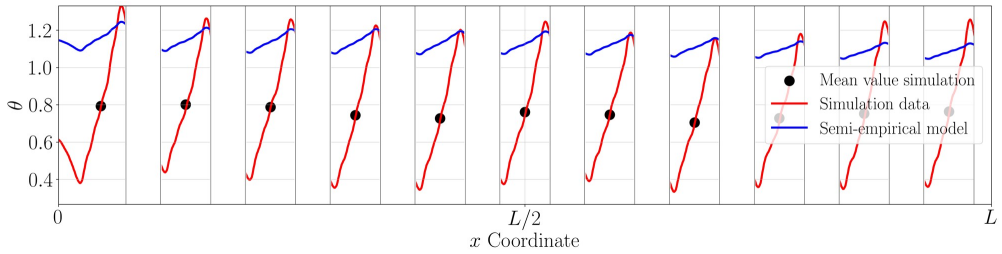

(c)

Fig. 10 Spatial distribution of the resistance component of impedance computed using the Dean's method along the face-sheet centerline. Tonal plane wave with amplitude equal to 145dB and tonal frequency equal to (a) 800 Hz, (b) 1400 Hz and (c) 2000 Hz. Turbulent grazing flow with centerline Mach number equal to 0.32.

The spatial distribution of reactance shows strong similarities to the resistance one. The variation of reactance within each cavity is about 0.2 for the acoustic wave with frequency equal to 800 Hz and about 0.4 for the other two frequencies. Reactance values obtained using the semi-empirical methods are within the range of the ones estimated from the numerical simulations and on the high-end side of the latter. Differently from resistance, a local peak in reactance is found at approximately the center of the cavity, and it corresponds to the location where the prediction from the semi-empirical model is close to the value provided by the numerical simulations. It is also important to notice that for the reactance the mean value and the semi-empirical model are very close for the lowest frequency investigated,

while for the other two, as for the resistance, the semi-empirical model predicts values higher than the one obtained using the numerical data.

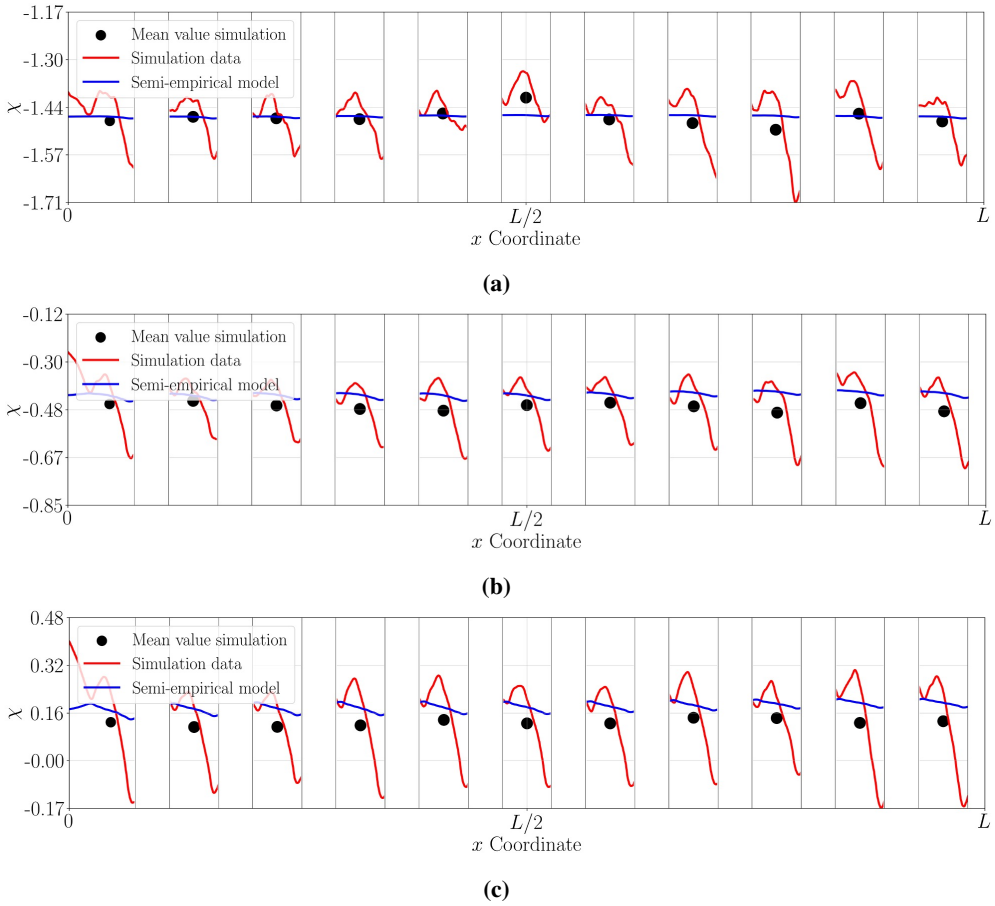

Fig. 11 Spatial distribution of the reactance component of impedance computed using the Dean's method along the face-sheet centerline. Tonal plane wave with amplitude equal to 145dB and plane wave with tonal frequency equal to (a) 800 Hz, (b) 1400 Hz and (c) 2000 Hz. Turbulent grazing flow with centerline Mach number equal to 0.32.

The analysis continues with the comparison between all the methods introduced previously. Figures 12 and 13 show both components of impedance for acoustic wave amplitude equal to 130 dB and 145 dB, respectively. Resistance and reactance values obtained from both the simulations, experiments [25] and the semi-empirical model [39] are presented. The description of the symbols present in each figure is the same as for the no grazing flow case.

For both cases, strong similarities between experiments and simulations are found. Starting with the resistance component, it can be noticed that the value predicted by the semi-empirical model is within the one provided by all the methods. The ones obtained with the Deans' method, at the probe location, are always lower that the ones provided by the eduction methods. Furthermore, based on the results shown in Figure 10, the average value of the resistance is almost constant on the entire face-sheet, therefore the average impedance obtained with the Dean's method differs from the average one obtained with the eduction techniques. However, the highest values of resistance on the face-sheet are similar to the ones obtained with the eduction methods. Focusing on the eduction methods, it can be observed that resistance obtained by the KT and Pierce's equation-based method differs from the experimental one at 800 Hz, and this is attributed to the short length of the liner with respect to the wavelength. It is important to notice that, when using data from the numerical simulations, even if the KT and the Pierce's equation-based method use both virtual microphones located along the liner section the first underestimates the resistance while the latter overestimates it. Conversely, the resistance obtained by Pierce's equation-based method calculated with a wall-normal uniform flow is slightly underestimated. At this frequency, on the other hand, resistance obtained with the MM method is closer to the

experimental one. At 1400 Hz, resistance values obtained with methods agree well with the experimental ones. The Pierce's equation-based method shows a slightly higher value both with the wall-normal uniform flow and a mean one. At 2000 Hz, values of educed impedance from the simulations with the KT and MM are similar but lower than the experimental ones, while the ones obtained with the Pierce's equation-based method are similar to the experimental educed ones. In this case, values obtained from the numerical simulations are close to the semi-empirical prediction. The only large discrepancy is found for the Pierce's equation-based method at 800 Hz and SPL equal to 145 dB.

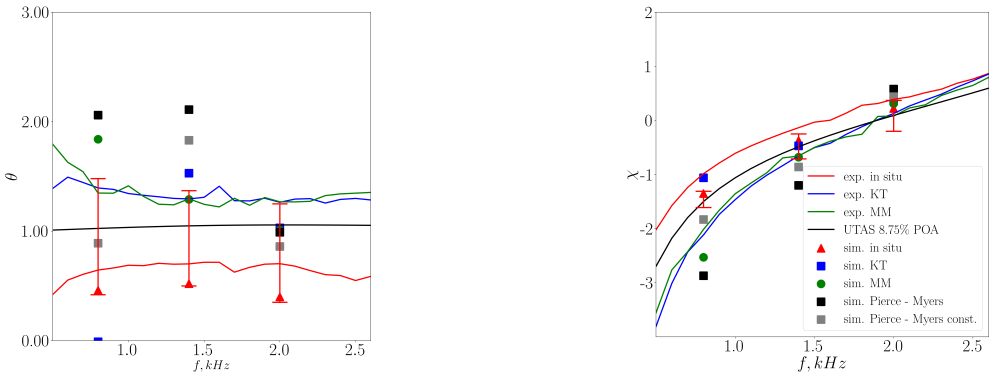

(a) **(b)**

Fig. 12 Comparison of (a) resistance and (b) reactance component of impedance for acoustic wave amplitude equal to 130 dB. Turbulent grazing flow with centerline Mach number equal to 0.32.

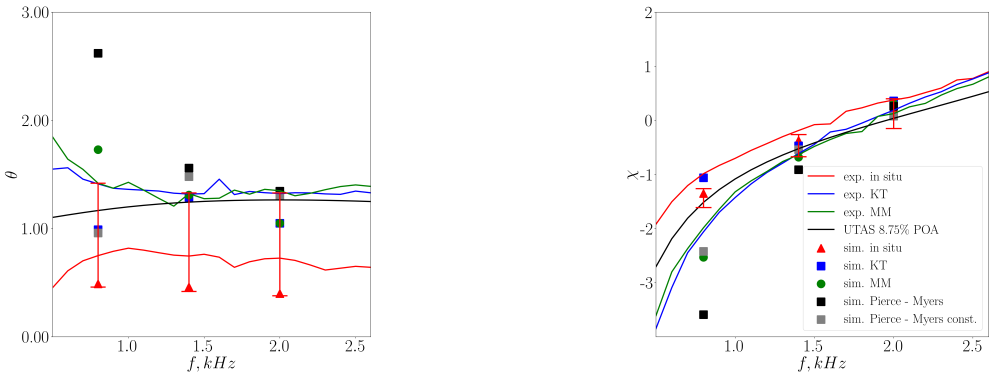

(a) **(b)**

Fig. 13 Comparison of (a) resistance and (b) reactance component of impedance for acoustic wave amplitude equal to 145 dB. Turbulent grazing flow with centerline Mach number equal to 0.32.

The analysis of the reactance also provides interesting insights. As a matter of fact, in this case, it is possible to observe that, also for this quantity, the values predicted by the semi-empirical method are within the ones obtained by the Deans' method and the eduction methods and that a good agreement between experiments and simulation is visible. As previously, the major discrepancy is found for the value of reactance obtained by the KT method at 800 Hz. Reactance values obtained with the different methods tend to collapse at higher frequencies but they differ at the lower one with the Deans' method showing higher values than the eduction methods. On the other hand, reactance values obtained with eduction methods are very similar.

To further understand the differences between the experiments and simulations for the KT method the decay of the SPL along the liner is plotted in Figure 14 for the acoustic wave with amplitude equal to 145 dB. For the sake of comparison, the SPL is normalized with respect to the SPL at beginning of the liner named SPL_{max}. In each subfigure, two experimental SPL decays are plotted: one refers to the one measured using the entire liner and the other is obtained by covering the liner face-sheet such to have the same number of cavities between experiments and simulations. The figure highlights, the impact of liner length on the SPL decay. Furthermore, it can be observed that the largest differences

between experiments and simulations are present at the end of the lined section. The figure also shows that for the case at 800 Hz, because of the short liner length in the numerical simulations there is absence of a clear decay of SPL, which can explain the large difference shown above.

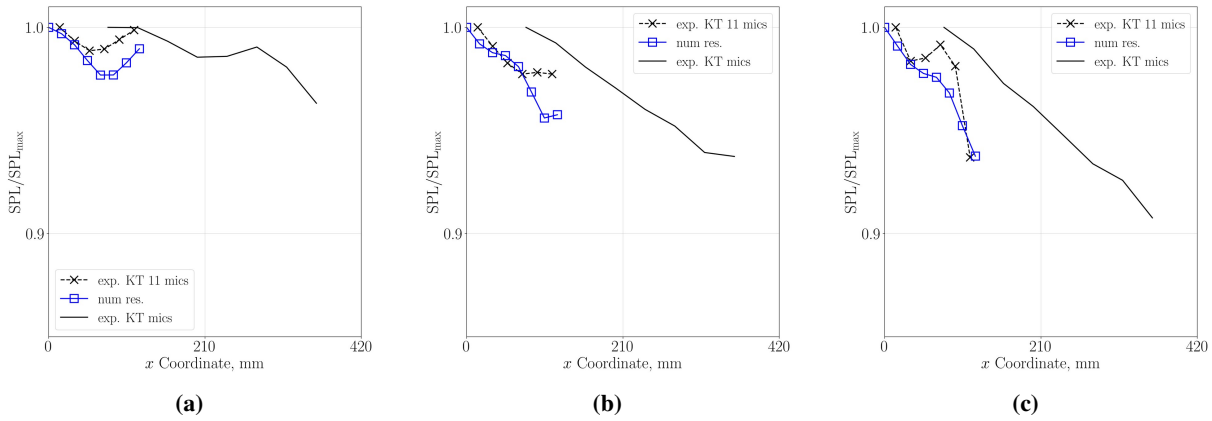

Fig. 14 Comparison of the SPL decay along the liner sample for acoustic wave amplitude equal to 145 dB and frequencies equal to (a) 800 Hz, (b) 1400 Hz and (c) 2000 Hz. Experimental values are obtained using the entire liner and covering part of it such to have the same number of cavities as in the simulations.

The analysis in the presence of the grazing flow continues with the comparison between upstream and downstream acoustic source for both amplitudes of the acoustic wave. Figure 15 shows resistance and reactance values, compared against the experimental ones, for acoustic source with amplitude equal to 130 dB. The same quantities for the case with acoustic amplitude equal to 145 dB are shown in Figure 16. As above, for the in-situ method, the symbol represents the local value taken using a virtual probe at the same location as the experimental one, while the bar represents the minimum and maximum values over the entire face-sheet. Furthermore, for the in-situ method the virtual probe for upstream and downstream case is located on the first cavity with respect to the direction of propagation of the acoustic wave, i.e., the first cavity for upstream source and the last cavity for the downstream one.

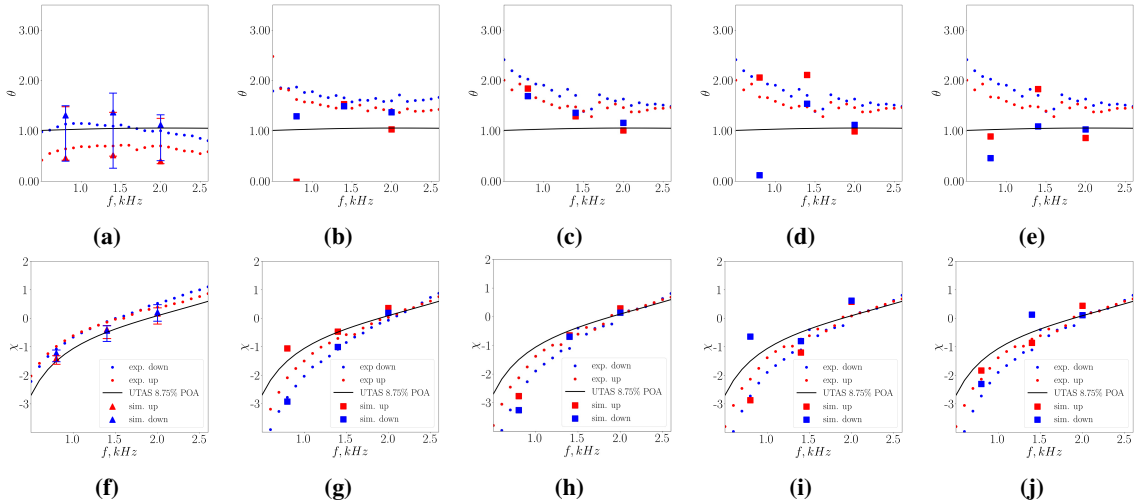

Fig. 15 Comparison of resistance (a-e) and reactance (f-j) values obtained for upstream and downstream acoustic wave with amplitude equal to 130 dB. Four methods to obtain impedance: (a, f) in-situ, (b, g) KT (c, h) MM, (d, i) Pierce and (e, j) Pierce with a wall-normal uniform flow.

For both amplitudes, the trend is that there is higher resistance and a lower reactance for the downstream source with respect to the upstream one. Differences between the methods exist. Starting from the resistance values, the in-situ method shows the largest differences between upstream and downstream source both in the experiments and simulations.

However, simulations results show that the variation of resistance over the entire face-sheet is very similar for both directions. Only Pierce's equation-based method does not show a clear trend. The reasons for this behaviour will be further investigated in the future. For the eduction methods, smaller differences are present between the two directions of propagation. These differences are less evident in the numerical simulations for the lowest amplitude investigated, while they are similar to the experimental ones for the highest one. Also in this case, it is possible to observe that, the highest values of resistance obtained using the Deans' method are close to the resistance values educed with KT and MM methods.

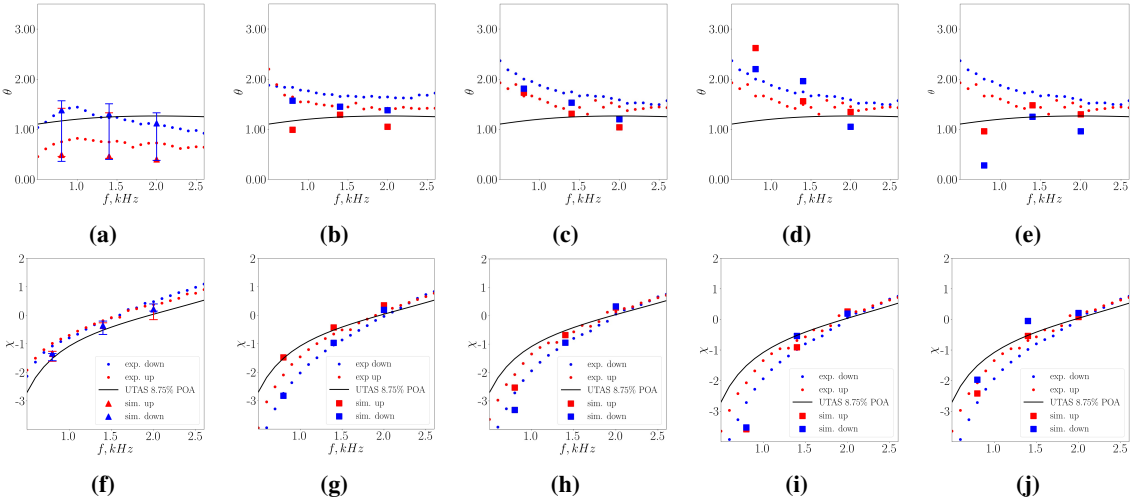

Fig. 16 Comparison of resistance (a-e) and reactance (f-j) values obtained for upstream and downstream acoustic wave with amplitude equal to 145 dB. Four methods to obtain impedance: (a, f) in-situ, (b, g) KT (c, h) MM, (d, i) Pierce and (e, j) Pierce with wall-normal uniform flow.

Moving to the reactance values, it is possible to observe that the ones obtained with the Deans' method, for both directions of propagation, are very similar in both the experiments and simulations, with small differences only at frequencies higher than 2000 Hz. On the other hand, both simulations and experiments show higher reactance values for the upstream source with respect to the downstream one and values that become very similar at frequencies higher than 2000 Hz. The educed reactance values for the KT and MM methods are always smaller than the one obtained with in-situ approach despite the spatial variability with the virtual probe locations. Despite the numerical data point at the lowest frequency for the KT method, the differences between upstream and downstream are similar to the one found in the experiments. Also, in this case, Pierce's equation-based method does not show a clear trend. The reasons will be better investigated in future analysis.

V. Conclusions

A comparison between different approaches to obtain impedance is presented. A numerical database is used as input. Eduction methods, based on the MM, KT and Pierce's equation, are compared with semi-empirical models and values obtained with the Deans' method. Simulations with and without grazing flow Mach number equal to 0.3 and acoustic waves with two amplitudes, equal to 130 dB and 145 dB, and three frequencies equal to 800 Hz, 1400 Hz and 2000 Hz are analyzed. It is found that results obtained with the Deans' method are highly dependent on the sampling location with a very large scatter, up to 100% of the mean value. However, the highest values obtained with the Deans' method are close to the ones obtained with the eduction method. Reactance values are instead different showing higher values for the Deans' method with respect to the eduction ones. The comparison between the methods shows the same trends also when comparing acoustic waves propagating in the direction opposite to the mean flow. For this case, the difference in impedance between upstream and downstream propagating acoustic wave is found in both experiments and simulations.

The good agreement between the numerical database and the experiments allow to use these simulations to shed light on the physical mechanisms present when an acoustic wave and a turbulent flow interact over acoustic liners.

Acknowledgments

The work of F. Avallone and A. Paduano is co-funded by the European Union (ERC, LINING, 101075903). Views and opinions expressed are however those of the author(s) only and do not necessarily reflect those of the European Union or the European Research Council. Neither the European Union nor the granting authority can be held responsible for them. This work was partially supported by the AeroAcoustics Research Consortium (AARC). The AARC is a government-industry partnership supporting pre-competitive research for aircraft noise reduction. L.A. Bonomo, L.M. Pereira and J.A. Cordioli gratefully acknowledge funding from Conselho Nacional de Desenvolvimento Científico e Tecnológico (CNPq), project number 407583/2022-0. On behalf of L.A. Bonomo, this study was financed in part by the Coordenação de Aperfeiçoamento de Pessoal de Nível Superior – Brasil (CAPES) – Finance Code 001. L.M. Pereira acknowledges scholarship funding from CNPq. L.A. Bonomo also acknowledges CNPq scholarship number 402701/2022-4.

References

[1] Casalino, D., Hazir, A., and Mann, A., "Turbofan Broadband Noise Prediction Using the Lattice Boltzmann Method," *AIAA Journal*, Vol. 56, No. 2, 2017, pp. 1–20. https://doi.org/10.2514/1.J055674, URL https://arc.aiaa.org/doi/10.2514/1.J055674.

[2] Watson, W., and Jones, M., "Evaluation of wall boundary conditions for impedance eduction using a dual-source method," *18th AIAA/CEAS Aeroacoustics Conference (33rd AIAA Aeroacoustics Conference)*, American Institute of Aeronautics and Astronautics Inc., 2012, pp. 2012–2199. https://doi.org/10.2514/6.2012-2199.

[3] Watson, W., and Jones, M., "Validation of a new procedure for impedance eduction in flow," *16th AIAA/CEAS Aeroacoustics Conference (31st AIAA Aeroacoustics Conference)*, 2010, pp. 2010–3764. https://doi.org/10.2514/6.2010-3764.

[4] Elnady, T., Bodén, H., and Elhadidi, B., "Validation of an Inverse Semi-Analytical Technique to Educe Liner Impedance," *AIAA Journal*, Vol. 47, No. 2, 2009, pp. 2836–2844. https://doi.org/10.2514/1.41647, URL https://arc.aiaa.org/doi/abs/10.2514/1.41647.

[5] Piot, E., Primus, J., and Simon, F., "Liner impedance eduction technique based on velocity fields," *18th AIAA/CEAS Aeroacoustics Conference (33rd AIAA Aeroacoustics Conference)*, American Institute of Aeronautics and Astronautics Inc., 2012, pp. 2012–2198. https://doi.org/10.2514/6.2012-2198, URL http://arc.aiaa.orghttps://arc.aiaa.org/doi/abs/10.2514/6.2012-2198.

[6] Busse-Gerstengarbe, S., Richter, C., Thiele, F., Lahiri, C., Enghardt, L., Roehle, I., Ferrante, P., and Scofano, A., "Impedance Eduction Based on Microphone Measurements of Liners Under Grazing Flow Conditions," *AIAA Journal*, Vol. 50, No. 4, 2012, pp. 867–879. https://doi.org/10.2514/1.J051232, URL https://arc-aiaa-org.tudelft.idm.oclc.org/doi/abs/10.2514/1.J051232https://arc.aiaa.org/doi/abs/10.2514/1.J051232.

[7] Jing, X., Peng, S., and Sun, X., "A straightforward method for wall impedance eduction in a flow duct," *The Journal of the Acoustical Society of America*, Vol. 124, No. 1, 2008, p. 227. https://doi.org/10.1121/1.2932256, URL https://asa.scitation.org/doi/abs/10.1121/1.2932256.

[8] De Roeck, W., and Desmet, W., "Indirect acoustic impedance determination in flow ducts using a two-port formulation." *15th AIAA/CEAS Aeroacoustics Conference (30th AIAA Aeroacoustics Conference)*, American Institute of Aeronautics and Astronautics Inc., 2009, pp. 2009–3302. https://doi.org/10.2514/6.2009-3302.

[9] Santana, L., De Roeck, W., Desmet, W., and Ferrante, P., "Two-port indirect acoustic impedance eduction in presence of grazing flows," *17th AIAA/CEAS Aeroacoustics Conference 2011 (32nd AIAA Aeroacoustics Conference)*, 2011, pp. 2011–2868. https://doi.org/10.2514/6.2011-2868, URL https://arc.aiaa.org/doi/abs/10.2514/6.2011-2868.

[10] Dean, P., "An in situ method of wall acoustic impedance measurement in flow ducts," *Journal of Sound and Vibration*, Vol. 34, No. 1, 1974, pp. 97–IN6. https://doi.org/10.1016/S0022-460X(74)80357-3.

[11] Roncen, R., Méry, F., Piot, E., and Simon, F., "Statistical inference method for liner impedance eduction with a shear grazing flow," *AIAA Journal*, Vol. 57, No. 3, 2019, pp. 1055–1065. https://doi.org/10.2514/1.J057559, URL https://arc-aiaa-org.tudelft.idm.oclc.org/doi/abs/10.2514/1.J057559.

[12] Zhou, L., Bodén, H., Lahiri, C., Bake, F., Enghardt, L., Busse-Gerstengarbe, S., and Elnady, T., "Comparison of impedance eduction results using different methods and test rigs," *20th AIAA/CEAS Aeroacoustics Conference*, American Institute of Aeronautics and Astronautics Inc., 2014, pp. 2014–2955. https://doi.org/10.2514/6.2014-2955.

[13] Jones, M., Watson, W., and Parrott, T., "Benchmark data for evaluation of aeroacoustic propagation codes with grazing flow," *11th AIAA/CEAS Aeroacoustics Conference*, Vol. 1, Monterey, California, 2005, pp. 2005–2853. https://doi.org/10.2514/6.2005-2853, URL https://arc-aiaa-org.tudelft.idm.oclc.org/doi/abs/10.2514/6.2005-2853.

[14] Primus, J., Piot, E., and Simon, F., "An adjoint-based method for liner impedance eduction: Validation and numerical investigation," *Journal of Sound and Vibration*, Vol. 332, No. 1, 2013, pp. 58–75. https://doi.org/10.1016/J.JSV.2012.07.051.

[15] Aurégan, Y., Leroux, M., and Pagneux, V., "Measurement of liner impedance with flow by an inverse method," *10th AIAA/CEAS Aeroacoustics Conference*, Vol. 1, American Institute of Aeronautics and Astronautics Inc., Manchester, Great Britain, 2004, pp. 2004–2838. https://doi.org/10.2514/6.2004-2838, URL https://arc-aiaa-org.tudelft.idm.oclc.org/doi/abs/10.2514/6.2004-2838.

[16] Jones, M., Watson, W., and Nark, D., "Effects of Flow Profile on Educed Acoustic Liner Impedance," *16th AIAA/CEAS Aeroacoustics Conference*, American Institute of Aeronautics and Astronautics, Reston, Virigina, 2010, pp. 2010–3763. https://doi.org/10.2514/6.2010-3763, URL https://arc.aiaa.org/doi/10.2514/6.2010-3763.

[17] Jones, M. G., and Howerton, B. M., "Evaluation of Novel Liner Concepts for Fan and Airframe Noise Reduction," *22nd AIAA/CEAS Aeroacoustics Conference*, American Institute of Aeronautics and Astronautics, Reston, Virginia, 2016. https://doi.org/10.2514/6.2016-2787, URL https://arc.aiaa.org/doi/10.2514/6.2016-2787.

[18] Ingard, U., "Influence of Fluid Motion Past a Plane Boundary on Sound Reflection, Absorption, and Transmission," *The Journal of the Acoustical Society of America*, Vol. 31, No. 7, 1959, pp. 1035–1036. https://doi.org/10.1121/1.1907805.

[19] Myers, M. K., "On the acoustic boundary condition in the presence of flow," *Journal of Sound and Vibration*, Vol. 71, No. 3, 1980, pp. 429–434. https://doi.org/10.1016/0022-460X(80)90424-1.

[20] Khamis, D., and Brambley, E., "Viscous effects on the acoustics and stability of a shear layer over an impedance wall," *Journal of Fluid Mechanics*, Vol. 810, 2017, pp. 489–534. https://doi.org/10.1017/JFM.2016.737, URL https://www.cambridge.org/core/journals/journal-of-fluid-mechanics/article/viscous-effects-on-the-acoustics-and-stability-of-a-shear-layer-over-an-impedance-wall/13FD3DF780AC14612D9844732310F18D.

[21] Léon, O., Méry, F., Piot, E., and Conte, C., "Near-wall aerodynamic response of an acoustic liner to harmonic excitation with grazing flow," *Experiments in Fluids*, Vol. 60, No. 9, 2019, p. 144. https://doi.org/10.1007/s00348-019-2791-5, URL http://link.springer.com/10.1007/s00348-019-2791-5.

[22] Ferrante, P., De Roeck, W., Desmet, W., and Magnino, N., "Back-to-back comparison of impedance measurement techniques applied to the characterization of aero-engine nacelle acoustic liners," *Applied Acoustics*, Vol. 105, 2016, pp. 129–142. https://doi.org/10.1016/J.APACOUST.2015.12.004.

[23] Bake, F., Burgmayer, R., Schulz, A., Knobloch, K., Enghardt, L., and Jones, M., "IFAR liner benchmark challenge #1 – DLR impedance eduction of uniform and axially segmented liners and comparison with NASA results:," *International Journal of Aeroacoustics*, Vol. 20, No. 7, 2021, pp. 478–496. https://doi.org/10.1177/1475472X211023844, URL https://journals.sagepub.com/doi/full/10.1177/1475472X211023844.

[24] Jones, M., Nark, D., and Howerton, B., "Overview of liner activities in support of the international forum for aviation research," *25th AIAA/CEAS Aeroacoustics Conference, 2019*, 2019. https://doi.org/10.2514/6.2019-2599, URL https://arc.aiaa.org/doi/10.2514/6.2019-2599.

[25] Bonomo, L., Quintino, N., Cordioli, J., Avallone, F., Jones, M., Howerton, B., and Nark, D., "A Comparison of Impedance Eduction Test Rigs with Different Flow Profiles," *AIAA AVIATION 2023 Forum*, American Institute of Aeronautics and Astronautics, Reston, Virginia, 2023. https://doi.org/10.2514/6.2023-3346.

[26] Paduano, A., Pereira, L., Bonomo, L., Cordioli, J., Casalino, D., and Avallone, F., "On the impact of the acoustic wave direction on the in-orifice flow dynamics of an acoustic liner grazed by a turbulent flow," *30th AIAA/CEAS Aeroacoustics Conference*, 2024.

[27] Spillere, A., Bonomo, L., Cordioli, J., and Brambley, E., "Experimentally testing impedance boundary conditions for acoustic liners with flow: Beyond upstream and downstream," *Journal of Sound and Vibration*, Vol. 489, 2020, p. 115676. https://doi.org/10.1016/j.jsv.2020.115676, URL https://linkinghub.elsevier.com/retrieve/pii/S0022460X2030506X.

[28] Elnady, T., and Bodén, H., "An Inverse Analytical Method for Extracting Liner Impedance from Pressure Measurements," *10th AIAA/CEAS Aeroacoustics Conference*, American Institute of Aeronautics and Astronautics, Reston, Virigina, 2004. https://doi.org/10.2514/6.2004-2836.

[29] Bonomo, L., Quintino, N., Spillere, A., Murray, P., and Cordioli, J., "A comparison of in situ and impedance eduction experimental techniques for acoustic liners with grazing flow and high sound pressure level," *International Journal of Aeroacoustics*, Vol. 23, No. 1-2, 2024, pp. 60–83. https://doi.org/10.1177/1475472X231225629.

[30] Casalino, D., Santini, S., Genito, M., and Ferrara, V., "Rocket Noise Sources Localization Through a Tailored Beam-Forming Technique," *AIAA Journal*, Vol. 50, No. 10, 2012, pp. 2146–2158. https://doi.org/10.2514/1.J051479.

[31] Casalino, D., and Barbarino, M., "Optimization of a Single-Slotted Lined Flap for Wing Trailing-Edge Noise Reduction," *Journal of Aircraft*, Vol. 49, No. 4, 2012, pp. 1051–1063. https://doi.org/10.2514/1.C031561.

[32] Casalino, D., and Barbarino, M., "Stochastic Method for Airfoil Self-Noise Computation in Frequency Domain," *AIAA Journal*, Vol. 49, No. 11, 2011, pp. 2453–2469. https://doi.org/10.2514/1.J050773.

[33] Casalino, D., Barbarino, M., and Visingardi, A., "Simulation of Helicopter Community Noise in Complex Urban Geometry," *AIAA Journal*, Vol. 49, No. 8, 2011, pp. 1614–1624. https://doi.org/10.2514/1.J050774.

[34] Casalino, D., "Finite Element Solutions of a Wave Equation for Sound Propagation in Sheared Flows," *AIAA Journal*, Vol. 50, No. 1, 2012, pp. 37–45. https://doi.org/10.2514/1.J050772.

[35] Casalino, D., "Benchmarking of different wave models for sound propagation in non-uniform flows," *Procedia Engineering*, Vol. 6, 2010, pp. 163–172. https://doi.org/10.1016/j.proeng.2010.09.018.

[36] Cerizza, D., and Casalino, D., "An Indirect Impedance Eduction Process for Liners with Arbitrarily Complex Geometry," *AIAA AVIATION 2023 Forum*, American Institute of Aeronautics and Astronautics, Reston, Virginia, 2023. https://doi.org/10.2514/6.2023-4186.

[37] Casalino, D., and Genito, M., "Achievements in the numerical modeling of fan noise radiation from aero-engines," *Aerospace Science and Technology*, Vol. 12, No. 1, 2008, pp. 105–113. https://doi.org/10.1016/j.ast.2007.10.005.

[38] Casalino, D., Diozzi, F., Sannino, R., and Paonessa, A., "Aircraft noise reduction technologies: A bibliographic review," *Aerospace Science and Technology*, Vol. 12, No. 1, 2008, pp. 1–17. https://doi.org/10.1016/j.ast.2007.10.004, URL http://linkinghub.elsevier.com/retrieve/pii/S1270963807001162http://www.sciencedirect.com/science/article/pii/S1270963807001162.

[39] Yu, J., Ruiz, M., and Kwan, H.-W., "Validation of Goodrich Perforate Liner Impedance Model Using NASA Langley Test Data," *14th AIAA/CEAS Aeroacoustics Conference (29th AIAA Aeroacoustics Conference)*, American Institute of Aeronautics and Astronautics, Reston, Virigina, 2008. https://doi.org/10.2514/6.2008-2930.

[40] Jones, M., and Nark, D., "Partition Thickness Considerations for Additively Manufactured Acoustic Liners," Tech. rep., NASA Langley Research Center, 10 2023.